Proceedings of ASME Turbo Expo 2011
GT2011
June 6-10, 2011, Vancouver, British Columbia, Canada

GT2011-45849

MODAL AND AEROELASTIC ANALYSIS OF A COMPRESSOR BLISK CONSIDERING MISTUNING

Jens Nipkau
Rolls-Royce Deutschland
D-15827 Blankenfelde-Mahlow, Germany

Arnold Kühhorn
Chair of Structural Mechanics and Vehicle Vibrational Technology

Bernd Beirow
Chair of Structural Mechanics and Vehicle Vibrational Technology
Brandenburg University of Technology Cottbus, D-03046 Cottbus, Germany

ABSTRACT

Focussing on three basic blade modes the effect of the flow's influence on the forced response of a mistuned HPC-blisk is studied using a surrogate lumped mass model called equivalent blisk model (EBM). Both measured and intentionally allowed mistuning is considered to find out in principle if the flow contributes to a slowdown of blade displacements with increasing mistuning. In a first step the mechanical properties of the EBM are adjusted to a finite element model and known mistuning distributions given in terms of blade frequencies and damping. Taking into account the flow structure interaction CFD-computations are carried out in order to derive aerodynamic influence coefficients (AIC) which are used to describe the aerodynamic forces coming along with the motion of each blade in the flow. These aerodynamic forces can be included directly in the EBM equations of motion or alternatively be used to calculate aeroelastic eigenvalues from which additional equivalent aerodynamic elements representing the co-vibrating air mass as well as aerodynamic stiffening and damping effects are derived. Both kinds of EBM are applied to study the forced response at least in a qualitative manner aiming to demonstrate some basic effects at low computing time.

NOMENCLATURE

1F	first blade flap mode
1T	first blade torsion mode
1TL	first blade tramline mode
AIC	aerodynamic influence coefficients
CFD	computational fluid dynamics
DFT	discrete fourier transform
DOF	degree of freedom
E3E	Engine 3E (technology program)
EAE	equivalent aerodynamic element
EBM	equivalent blisk model
FE	finite element
FRF	frequency response function
FSI	fluid structure interaction
HPC	high pressure compressor
IBPA	inter blade phase angle
SDOF	single degree of freedom
$d_{a,i}$ [Ns/m]	discrete aerodynamic interblade damping
$d_{a,i}^{bas}$ [Ns/m]	discrete aerodynamic basic damping
d_b [Ns/m]	structural blade damping
d_{sec} [Ns/m]	structural sector damping
E [N/m²]	Young's modulus
f [Hz]	frequency
$\underline{f}$ [N]	complex modal force
f_{blade} [Hz]	blade alone frequency
j [-]	mode index, imaginary unit
$k_{a,i}$ [N/m]	discrete air stiffness contribution
$k_{b,i}$ [N/m]	stiffness of i^{th} blade
k_{sec} [N/m]	disk sector stiffness
k_c [N/m]	coupling stiffness
$\hat{\underline{L}}$ [N/m]	complex aerodynamic influence coefficient
m_b [kg]	effective blade mass
m_{sec} [kg]	disk sector mass
$\Delta m_{a,i}$ [kg]	co-vibrating air mass of i^{th} blade
N [-]	number of blades
p [N/m²]	static pressure
$q_0^{\psi}(t)$ $\left[\mathrm{m}\sqrt{\mathrm{kg}}\right]$	forced modal displacement of the reference blade (mass normalized)
V [-]	modulus of FRF
x_i [m]	displacement of i^{th} DOF

x_0 [m]	forced displacement of the reference blade
δ [1/s]	decay rate
ζ [-]	critical damping ratio
η [-]	frequency ratio
λ [1/s]	eigenvalue
φ [°]	IBPA of cyclic symmetric modes
ω [rad/s]	angular natural frequency
Ω [rad/s]	angular exciting frequency

Indices

0	reference blade
a	aerodynamic
b	blade
bas	basic
c	coupling
F	external force
i	blade index
j	mode index
sec	disk sector
φ	IBPA-dependence
Ψ	mass normalization
*	blisk sector with rigid disk

Vectors and Matrices

$\underline{\boldsymbol{F}}$	complex force vector
$\boldsymbol{n}$	normal vector
$\underline{\boldsymbol{D}}$	complex damping matrix
$\underline{\boldsymbol{K}}$	complex stiffness matrix
$\underline{\boldsymbol{M}}$	complex mass matrix
$\boldsymbol{\Psi}$	vector of mass-normalized mode shape

Note: Underlines indicate complex values

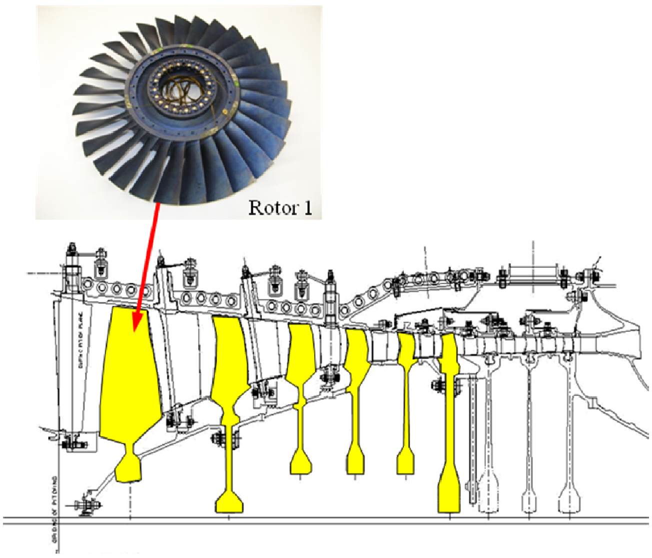

Figure 1 E3E-HPC Test-compressor [11]

1 INTRODUCTION

The analyses of turbomachinery components such as compressor rotors are widely based on simulations of perfectly tuned systems. However, due to deviations from the ideal design intention coming from tolerances of the manufacturing processes and/or material inhomogeneities respectively, a real turbomachinery rotor will always be mistuned no matter how small the tolerances may be. In this context, mistuning is referred to as the variation of mechanical properties of the rotor's blades. This variation expresses itself as varying blade eigenfrequencies and the splitting of the orthogonal modes of the slightly damped cyclic symmetric blisk system.

Compressor rotors manufactured as blisk, meaning the blades being an integral part of the disk, exhibit only little mechanical damping which is due to lack of friction at the contact faces of the blades' roots and the disk. During operation a blisk may face engine order excitation which, in the case of a mistuned system, may lead to so called mode localization and an increase of blade amplitudes between 20 and 402 % compared to the tuned response as shown among others in [1-10]. Whitehead [5] found an upper limit of blade displacement magnification of the forced response due to mistuning given by $1/2(1+\sqrt{N})$. In [9] a slowdown of the blade displacement magnification due to the flow could be shown. In [17] and [19] even a reduction of the forced response could be proved in case of large frequency mistuning. The following work addresses the problem within analyses of a real mistuned blisk. In this regard the forced response is computed considering experimental results and the fluid structure interaction.

Using the example of an E3E [11] high pressure compressor's first stage (Fig. 1), the results of experimental mistuning identification based on blade by blade measurements [10, 12], model updating [12] and the simulation of the aeroelastic behavior are presented. The update of the FE-Model with respect to the mistuning pattern shows very good correlation with experimental data and allows numerical analyses of the mistuned system. With the information of the blades' natural frequencies an aeroelastic computation using CFD is performed in order to obtain the aeroelastic eigenvalues along with the aerodynamic influence coefficients which represent the aerodynamic influence on the blades' vibrations.

Furthermore an Equivalent Blisk Model (EBM) is adapted to the mechanical properties of the compressor blisk [13] and intensive numerical analyses of the forced response behavior of the blisk are performed. Two different methods are employed to include aerodynamic effects in the EBM. One uses the aerodynamic influence coefficients [14-16] as derived from the aeroelastic computations while the other, alternative one uses the aeroelastic eigenvalues to determine equivalent aerodynamic mass-, damping- and stiffness-elements. Both methods are compared one another. Since both methods are based on low degree models they are well suited to perform sensitivity investigations. For example, intentional mistuning analyses are carried out to assess the consequences of increasing mistuning on the response amplification.

2 STRATEGY

The complete strategy how aeroelastic effects can be taken into account for a mistuned blisk is shown in Fig. 2. At the beginning blade by blade measurements are carried out in order to identify structural mistuning as introduced in [10] and [12]. Impact excitation is employed to each blade step by step applying a miniature hammer and the vibration velocity is measured at the same blade based on laser-Doppler-vibrometry. Aiming to isolate a blade dominated frequency in the particular FRF all blades except the excited one are detuned with additional mass elements to destroy the slightly disturbed cyclic symmetry of the mistuned blisk completely. As a result distributions of blade dominated frequencies are identified as given in a normalized manner for the j^{th} blade mode (Fig. 3) with

$$\Delta f_i = \frac{f_{j,i} - \bar{f}_j}{\bar{f}_j}. \tag{1}$$

Herein $\bar{f}_j$ represents the arithmetic mean value of N blade dominated frequencies $f_{j,i}$ (i = 1…N) belonging to the j^{th} blade mode. Mode 1 (j = 1) represents the fundamental flap mode (1F), Mode 3 (j = 3) the first torsion (1T) and Mode 6 (j = 6) the tramline mode (1 TL) describing a bending to the longitudinal blade axis (Fig 4).

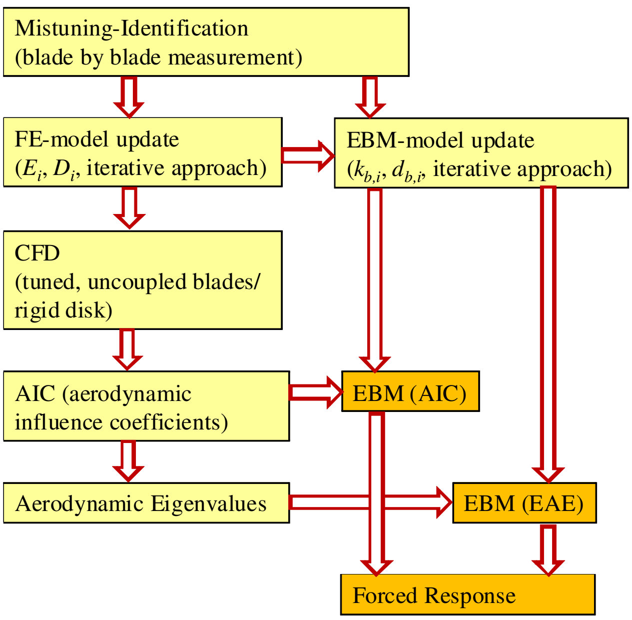

Figure 2 Strategy of approach

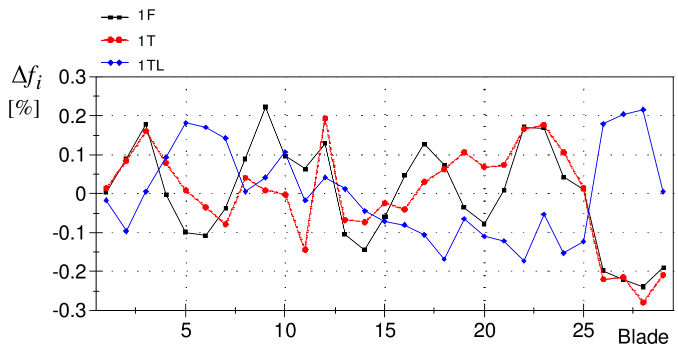

Figure 3 Normalized frequency mistuning distributions

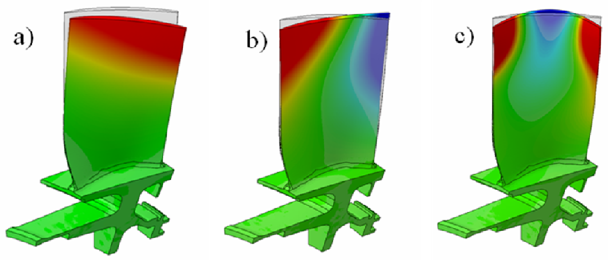

Figure 4 a) Mode 1 (1F) b) Mode 3 (1T) c) Mode 6 (1TL)

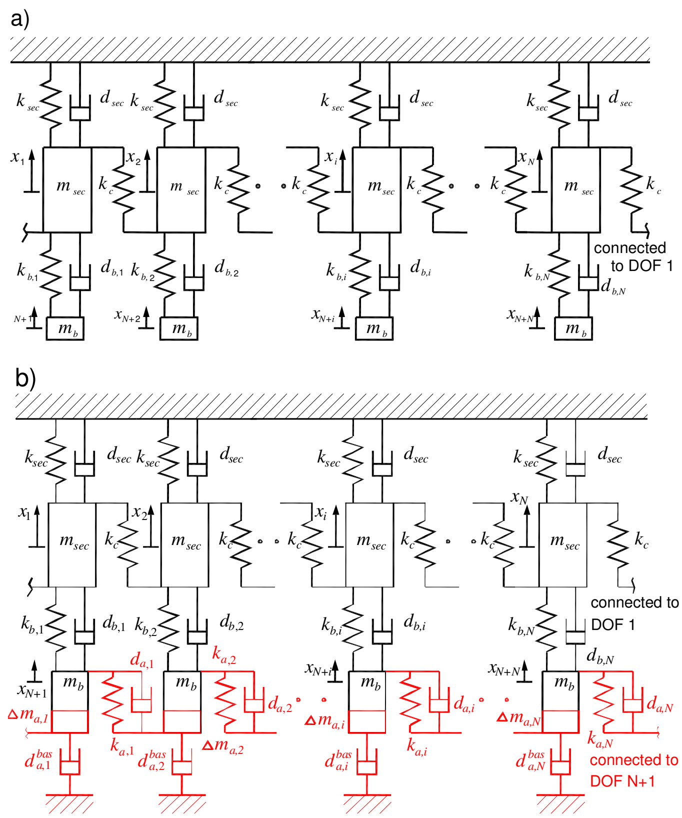

Figure 5 a) Structural EBM, b) EBM with additional equivalent aerodynamic elements (EAE)

In addition the damping ratios differing for each blade and each blade mode are measured. Following this experimental modal information is used to update both FE-Models of the blisk [12] and low degree of freedom models (one for each blade mode shape), the equivalent blisk models [13], which are composed of discrete masses, springs and dashpots (Fig 5a). The update of each model is based on an adjustment of both the stiffness (E_i or $k_{b,i}$) and the damping D_i of each blade in an iterative approach requiring that measured and calculated FRF coincide. Please note, that for each blade mode different EBM and FE-models have to be adjusted. In parallel, FSI-computations are carried out employing a commercial CFD-code aiming to derive aerodynamic influence coefficients (AIC). The AIC methodology, which has been introduced among others by Hanamura et al. [14], Kahl [15] and Kielb et al. [16], is implemented in the EBM with the objective to compute forced responses (see Section 6). As an alternative, aerodynamic eigenvalues computed with the AIC-technique are used to identify additional discrete equivalent aerodynamic elements (EAE) as displayed in Fig. 5b (see Section 5). Finally, the forced response results computed with both kinds of EBM are compared.

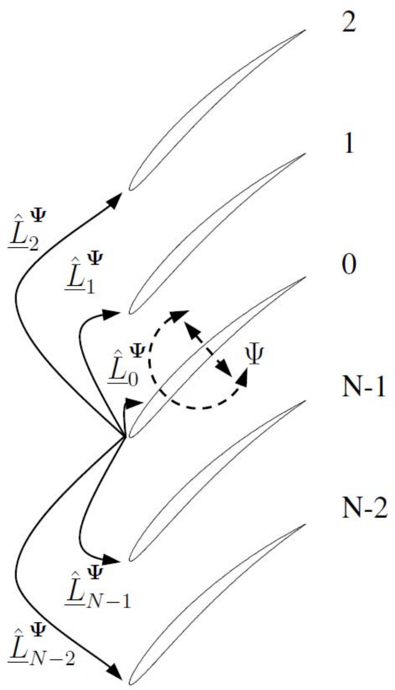

Figure 6 Scheme of aerodynamic influence coefficients

3 CALCULATION OF AERODYNAMIC INFLUENCE COEFFICIENTS

The method of aerodynamic influence coefficients (AIC) is a technique that considers the aerodynamic influences in blade individual coordinates. That means that the aerodynamic forces are not represented in travelling wave coordinates, but the aerodynamic coupling is regarded through coefficients only depending on the distance between the blades. How the methods works in principle is shown in Fig. 6.

Aiming to determine the influence coefficients only one reference blade (blade no. 0, Fig. 6) in an assembly of N blades and a rigid disk is forced to perform a sine-shaped vibration in a particular mass normalized mode shape $\boldsymbol{\Psi}$ with

$$x_0(t) = \boldsymbol{\Psi} q_0^{\Psi}(t)\,. \tag{1}$$

Consequently, the blade motion induces flow perturbations on the reference blade as well as on the rest of the blades in the assembly. Naturally, the influences and thus the strength of the disturbances decrease with increasing distance from the reference blade. The modal force acting on each blade i due to the reference blade motion can be calculated by

$$\underline{f}_i^{\boldsymbol{\Psi}}(t) = \int_A \underline{p}_i(t)\boldsymbol{\Psi}\boldsymbol{n}_i dA_i\,, \tag{2}$$

whereat $\underline{p}_i(t)$ represents the unsteady static pressure and $\boldsymbol{n}_i$ is the normal vector of the area element dA_i. The corresponding complex influence coefficient is calculated by means of

$$\hat{\underline{L}}_i^{\boldsymbol{\Psi}}(t) = \frac{\hat{\underline{f}}_i^{\boldsymbol{\Psi}}}{\hat{q}_0^{\boldsymbol{\Psi}}} \tag{3}$$

with $\hat{\underline{f}}_i^{\boldsymbol{\Psi}}$ being the complex modal force amplitude and $\hat{q}_0^{\boldsymbol{\Psi}}$ being the modal displacement of the reference blade. The influence coefficients are inserted into the complex influence coefficient matrix (dimension $2N$ x $2N$)

$$\hat{\underline{\boldsymbol{L}}}^{\boldsymbol{\Psi}} = \left[\begin{array}{cccc|cccc}
0 & 0 & \cdots & 0 & 0 & 0 & \cdots & 0 \\
0 & 0 & \ddots & \vdots & 0 & 0 & \ddots & \vdots \\
\vdots & \ddots & \ddots & 0 & \vdots & \ddots & \ddots & 0 \\
0 & \cdots & 0 & 0 & 0 & \cdots & 0 & 0 \\
\hline
0 & 0 & \cdots & 0 & \hat{\underline{L}}_0^{\boldsymbol{\Psi}} & \hat{\underline{L}}_{N-1}^{\boldsymbol{\Psi}} & \cdots & \hat{\underline{L}}_1^{\boldsymbol{\Psi}} \\
0 & 0 & \ddots & \vdots & \hat{\underline{L}}_1^{\boldsymbol{\Psi}} & \hat{\underline{L}}_0^{\boldsymbol{\Psi}} & \hat{\underline{L}}_{N-1}^{\boldsymbol{\Psi}} & \cdots \\
\vdots & \ddots & \ddots & 0 & \cdots & \hat{\underline{L}}_1^{\boldsymbol{\Psi}} & \hat{\underline{L}}_0^{\boldsymbol{\Psi}} & \hat{\underline{L}}_{N-1}^{\boldsymbol{\Psi}} \\
0 & \cdots & 0 & 0 & \hat{\underline{L}}_{N-1}^{\boldsymbol{\Psi}} & \cdots & \hat{\underline{L}}_1^{\boldsymbol{\Psi}} & \hat{\underline{L}}_0^{\boldsymbol{\Psi}}
\end{array}\right]. \tag{4}$$

In (4) only the coefficients acting on blades' DOF differ from zero. By means of the influence coefficients matrix the EBM equation of motion is given with

$$\underline{\boldsymbol{M}}\,\ddot{\underline{\boldsymbol{x}}}(t) + \underline{\boldsymbol{D}}\,\dot{\underline{\boldsymbol{x}}}(t) + \underline{\boldsymbol{K}}\,\underline{\boldsymbol{x}}(t) = \hat{\underline{\boldsymbol{L}}}^{\boldsymbol{\Psi}} \cdot m_b\,\underline{\boldsymbol{x}}(t) + \underline{\boldsymbol{F}}^F(t) \tag{5}$$

Herein the matrices $\underline{\boldsymbol{M}}$, $\underline{\boldsymbol{D}}$ and $\underline{\boldsymbol{K}}$ are written in complex notation although they are real quantities. $\underline{\boldsymbol{F}}^F$ is the complex vector of external excitation forces, $\ddot{\underline{\boldsymbol{x}}}(t)$, $\dot{\underline{\boldsymbol{x}}}(t)$ and $\underline{\boldsymbol{x}}(t)$ denote the complex acceleration, velocity and displacement response vectors. The effective blade mass m_b (real number) acts as a scaling factor to consider the mass normalization of $\boldsymbol{\Psi}$.

4 AEROELASTIC EIGENVALUES

Aiming at a determination of the aeroelastic eigenvalues the mechanical damping matrix $\underline{\boldsymbol{D}}$ as well as the external forces $\underline{\boldsymbol{F}}^F$ in Eq. (5) are set to zero. Note, that the dimension of the matrices is reduced to N x N, since the aeroelastic eigenvalues have to be computed for a rigid disk as assumed in the derivation of the AIC. In consequence the homogeneous eigenvalue problem can be written as

$$\left\{\lambda_a^2 \underline{\boldsymbol{M}} + \left[\underline{\boldsymbol{K}} - \hat{\underline{\boldsymbol{L}}}\right]\right\}\hat{\boldsymbol{x}} = \boldsymbol{0} \tag{6}$$

with

$$\hat{\underline{\boldsymbol{L}}} = \hat{\underline{\boldsymbol{L}}}^{\boldsymbol{\Psi}} \cdot m_b \tag{7}$$

and

$$\lambda_a = -\delta_a + j\omega_a \tag{8}$$

naming the aeroelastic eigenvalue λ_a containing the aerodynamic damping described with the decay rate δ_a and the angular aerodynamic natural frequency $\omega_{a,i}$. The solution of Eq. (6) yields the N aeroelastic eigenvalues $\lambda_{a,i}$ from which the critical aerodynamic damping ratio $\zeta_{a,i}$ by means of the structural angular natural frequency $\omega_{0,i}$

$$\zeta_{a,i} = \frac{\delta_{a,i}}{\omega_{0,i}} = \frac{\mathrm{Re}\{\lambda_{a,i}\}}{\sqrt{\mathrm{Re}\{\lambda_{a,i}\}^2 + \mathrm{Im}\{\lambda_{a,i}\}^2}} \tag{9}$$

and

$$\omega_{a,i} = \mathrm{Im}\{\lambda_{a,i}\} \tag{10}$$

can be calculated. For a validation of the strategy using the AIC-technique to calculate aeroelastic eigenvalues please refer to [17] where AIC-results are well correlated to those obtained with uni- and bidirectionally coupled FSI-computations.

5 CALCULATION OF EQUIVALENT AERODYNAMIC ELEMENTS

The aeroelastic eigenvalues given in the previous section are used to derive the equivalent aerodynamic elements as shown in Fig 5b. In detail these are the co-vibrating air-masses $\Delta m_{a,i}$, discrete aerodynamic springs $k_{a,i}$ to consider the stiffening or the softening affecting adjacent blades due to the flow and aerodynamic dashpots, which are divided into a basic part $d_{a,i}^{bas}$ connecting a blade to the ground and a part $d_{a,i}$ acting between adjacent blades. Except the basic damping part, all parameters are defined to be interblade phase angle (IBPA)-dependent. The IBPA is defined as phase difference between adjacent blades. Considering one blisk sector and using the aeroelastic parameters as basis, the equivalent aerodynamic parameters (EAE) can be calculated. Since the aeroelastic eigenvalues have been calculated for the tuned case, this means that cyclic symmetry conditions are valid and the blade parameters are same for the entire blade assembly: $m_{b,i} = m_b$, $d_{b,i} = d_b = 0$ and $k_{b,i} = k_b$. The equation of motion can be written as

$$m_\varphi^* \ddot{x}_i + d_\varphi^* \dot{x}_i + k_\varphi^* x_i = 0 \tag{11}$$

with

$$m_\varphi^* = \Delta m_{a,\varphi} + m_b \,, \tag{12}$$

$$d_\varphi^* = d_a^{bas} + 2d_{a,\varphi}(1-\cos\varphi) \tag{13}$$

and

$$k_\varphi^* = k_b + 2k_{a,\varphi}(1-\cos\varphi)\,. \tag{14}$$

Details for the derivation of Eqn. (11)-(14) are given in Annex A. The IBPA-individual eigenvalues assigned to Eq. (11) are

$$\lambda_{\varphi 1,2} = -\zeta_\varphi^* \omega_{0,\varphi}^* \pm i\omega_{0,\varphi}^* \sqrt{1-\zeta_\varphi^{*2}} = \mathrm{Re}_\varphi^* \pm i\,\mathrm{Im}_\varphi^* \tag{15}$$

whereat

$$\zeta_\varphi^* = \frac{-\mathrm{Re}_\varphi^*}{\omega_{0,\varphi}^*} = \frac{d_\varphi^*}{2m_\varphi^* \omega_{0,\varphi}^*} = \frac{d_a^{bas} + 2d_{a,\varphi}(1-\cos\varphi)}{2\sqrt{(\Delta m_{a,\varphi} + m_b)(d_a^{bas} + 2k_{a,\varphi}(1-\cos\varphi))}}\,, \tag{16}$$

$$\omega_\varphi^* = \mathrm{Im}_\varphi^* = \sqrt{\frac{k_b + 2k_{a,\varphi}(1-\cos\varphi)}{(\Delta m_{a,\varphi} + m_b)}}\sqrt{1-\zeta_\varphi^{*2}} \tag{17}$$

and

$$\omega_{0,\varphi}^* = \sqrt{\mathrm{Im}_\varphi^{*2} + \mathrm{Re}_\varphi^{*2}}\,. \tag{18}$$

Since $\omega_{0,\varphi}^*$ as well as ζ_φ^* are known quantities from the calculation of the aeroelastic eigenvalues presented in Section 4 ($\omega_{0,\varphi}^* = \omega_{0,i}$ and $\zeta_\varphi^* = \zeta_{a,i}$) the modulus of the FRF can be calculated according to

$$V_\varphi^* = \frac{1}{\sqrt{(1-\eta_\varphi^{*2})^2 + 4\zeta_\varphi^{*2}\eta_\varphi^{*2}}} \tag{19}$$

with the ratio of the angular exciting frequency Ω and the undamped angular natural frequency $\omega_{0,\varphi}^*$

$$\eta_\varphi^* = \frac{\Omega}{\omega_{0,\varphi}^*}\,. \tag{20}$$

Hence the stiffness k_φ^* can be calculated according as

$$k_\varphi^* = \frac{\hat{f}_\varphi V_\varphi^*}{\hat{x}_0} m_b\,. \tag{21}$$

The amplitudes of the modal force $\hat{f}_\varphi$ and the displacement $\hat{x}_0$ of the reference blade are known from the FSI-computations, the scaling with m_b considers the mass normalization of $\boldsymbol{\Psi}$.

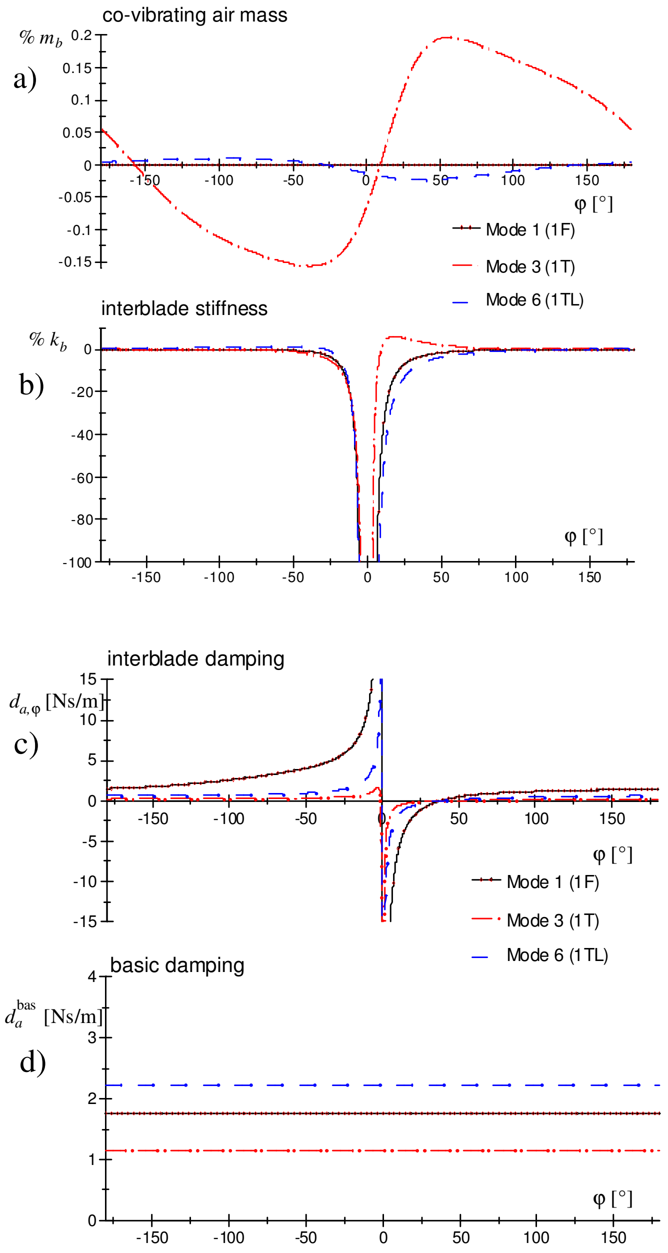

Figure 7: Calculated EAE: a) $\Delta m_{a,\varphi}$ b) $k_{a,\varphi}$ c) $d_{a,\varphi}$ d) d_a^{bas}

With the from now on known stiffness k_φ^* the IBPA-dependent stiffness

$$k_{a,\varphi} = \frac{k_\varphi^* - k_b}{2(1-\cos\varphi)} \quad \text{for } \varphi \neq 0° , \qquad (22)$$

$$m_\varphi^* = \frac{k_\varphi^*}{\omega_{0,\varphi}^{*2}} \qquad (23)$$

and finally

$$\Delta m_{a,\varphi} = m_\varphi^* - m_b \qquad (24)$$

can be computed. If one assume a constant basic damping as given with

$$d_a^{bas} = 2\zeta_{\varphi=0°}^* \sqrt{k_b(\Delta m_{a,\varphi=0°} + m_b)} , \qquad (25)$$

the last unknown parameter, the IBPA-dependent damping can be calculated according to

$$d_{a,\varphi} = \frac{2\zeta_\varphi^* \sqrt{m_\varphi^* k_\varphi^*}}{2(1-\cos\varphi)} \quad \text{with } \varphi \neq 0° . \qquad (26)$$

In Fig. 7 the results of the EAE-calculation are displayed. It is conspicuous that the curves of both the inter-blade stiffness and inter blade damping (Figs. 7d and 7c) are characterized by poles close to an inter blade phase angle of zero which results from the structure of Eqn. (22) and (26) used to calculate these parameters. However, in case of low inter blade phase angles the relative motion of adjacent blades also takes low values so that the resulting aerodynamic forces are limited. An extreme case is represented by an IBPA of φ = 0° where no relative motion of blades occurs and hence neither mechanical work nor aerodynamic forces are contributed from inter blade springs and dashpots even if stiffness and damping coefficients (Figs. 7b and 7c) take high values. Negative damping coefficients appearing in Fig. 7c between φ = 0° and φ = 35° contribute to an amplification of the response. Considering the co-vibrating air mass (Fig. 7a), quantities below 0.2 % of the effective structural blade mass can be found. In case of Mode 1, the contribution of it is negligibly small. The basic damping (Fig. 7d) takes constant values as assumed in Eq. (25).

6 FORCED RESPONSE

In a first step, the ideally tuned blisk is used to carry out the forced response computations. A unit travelling wave excitation acting on each blade is employed whereas both forward and backward travelling waves are considered. Since the blisk has 29 blades this means that results due to engine orders (EO) ranging from 0 to 28 have to be calculated. The EOs 15 to 28 correspond to the alias EOs -1 to-14 representing backward travelling waves. Both the EBM based on AIC and the EBM based on EAE are used to compute the forced response.

Results of the computation are displayed in Fig. 8 showing curves of normalized maximum displacements and related frequencies which are normalized with the blade alone frequency f_{blade} of the mode considered. In case of the blade Mode 1 (Fig 8a) a good match of the AIC- and EAE-calculated displacements and, apart from EO 0, of frequencies can be found.

With respect to Modes 3 and 6 (Fig. 8 b, c) the correlation of frequencies is excellent. However, larger deviations of up to 25 % occur as to the displacements especially close to the alias EO -4 and -5 where a strong change of maximum frequency is apparent.

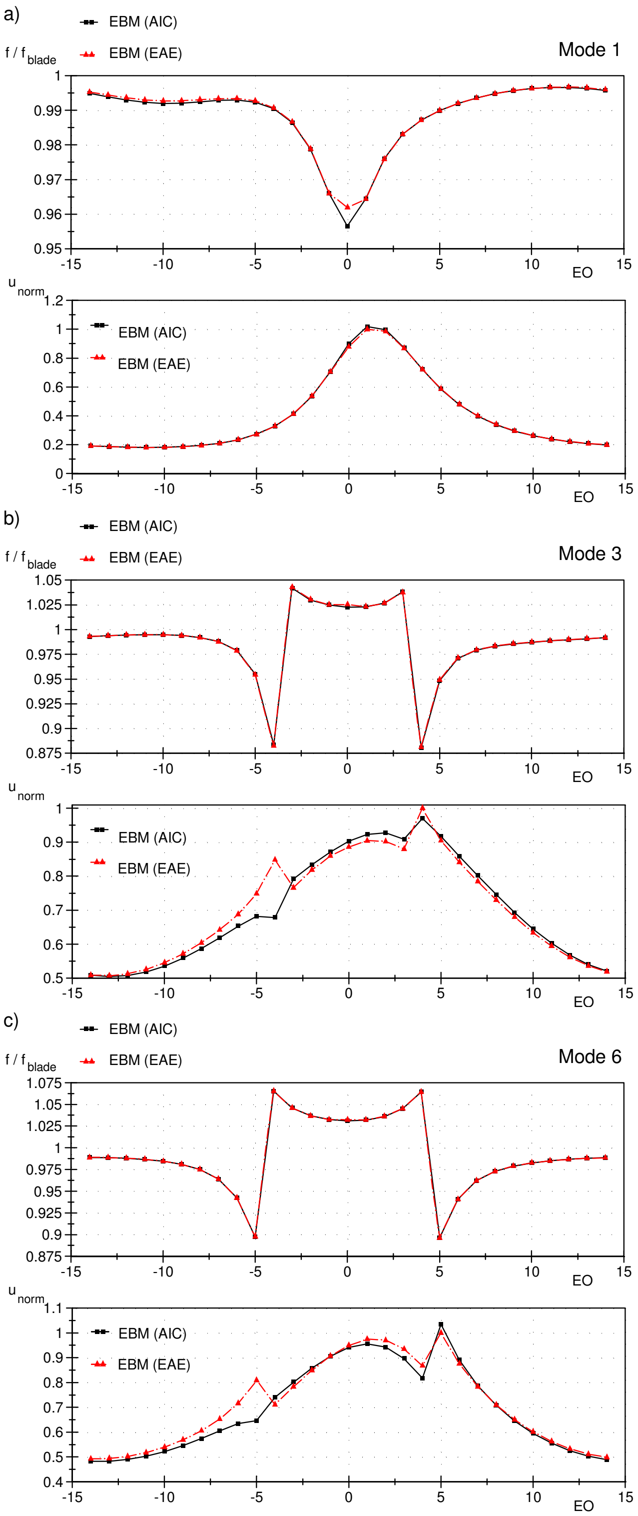

Figure 8: Maximum forced response of the tuned blisk
a) Mode 1 b) Mode 3 c) Mode 6

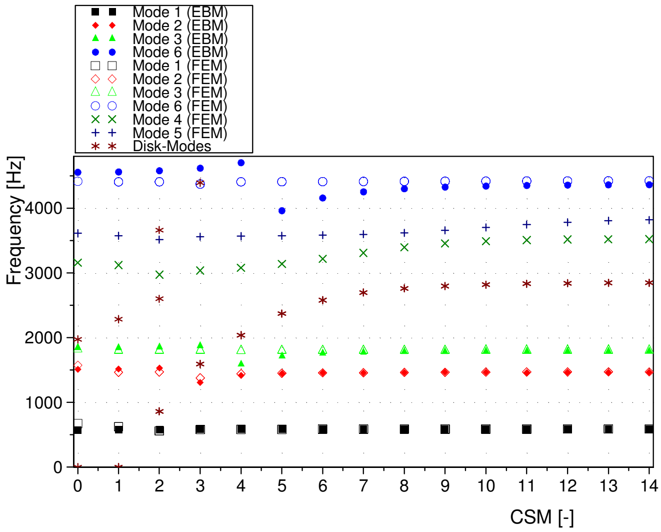

Figure 9: Nodal diameter chart (in vacuum blisk)

It has to be emphasized that in regions with clearly changing natural frequencies an increasing degree of blade-disk-coupling has a major influence on the accuracy of the EBM (Fig. 9) and hence, on the forced response analyses. The simplicity of the modeling leads to an in-phase motion of blades and disk sectors connected to them for EOs ranging from -4 to +4 whereas an out of phase motion occurs for other EO-excitations. Nevertheless, the AIC-results considering a direct aerodynamic coupling between all blades can be regarded as the more realistic approach. For other EOs being not equal then EO -4 and -5 the deviation of displacements ranges from 0 to 6 % (Fig. 8 b, c).

Relevant engine orders with regard to the real engine operation are amongst others the EOs 2, 7 and 14. If a mistuned blisk is analyzed, an iterative computation is required in case of an EAE-approach since IBPA are not constant as they are for a tuned blisk. Hence, a new allocation of aerodynamic elements is necessary after each iteration loop.

Considering the FRF of a Mode 1 excitation with EO 7 an excellent agreement of AIC- and EAE-computations also close to the resonance is apparent (Fig. 10a). Even for the mistuned blisk the deviation clearly remains below 0.01 %. Larger deviations in resonance occur in case of Mode 3 and EO 2 (Fig. 10b) with 2.8 % considering a tuned blisk and even 7.3 % considering a mistuned blisk. For the tramline-mode (Fig. 10c) excited with EO 14 we get 1.7 % (tuned) and 2.1 % (mistuned). With respect to the resonance frequencies the differences are ranging from 0 to 0.06 %. One explanation for the bigger differences of the mistuned blisk could be that due to mistuning one get differing eigenvalues compared to those obtained for a tuned system, which has been used to derive the equivalent aerodynamic elements. Furthermore, the aerodynamic coupling of blade motions is limited to immediately adjacent blades if the EAE-technique is employed.

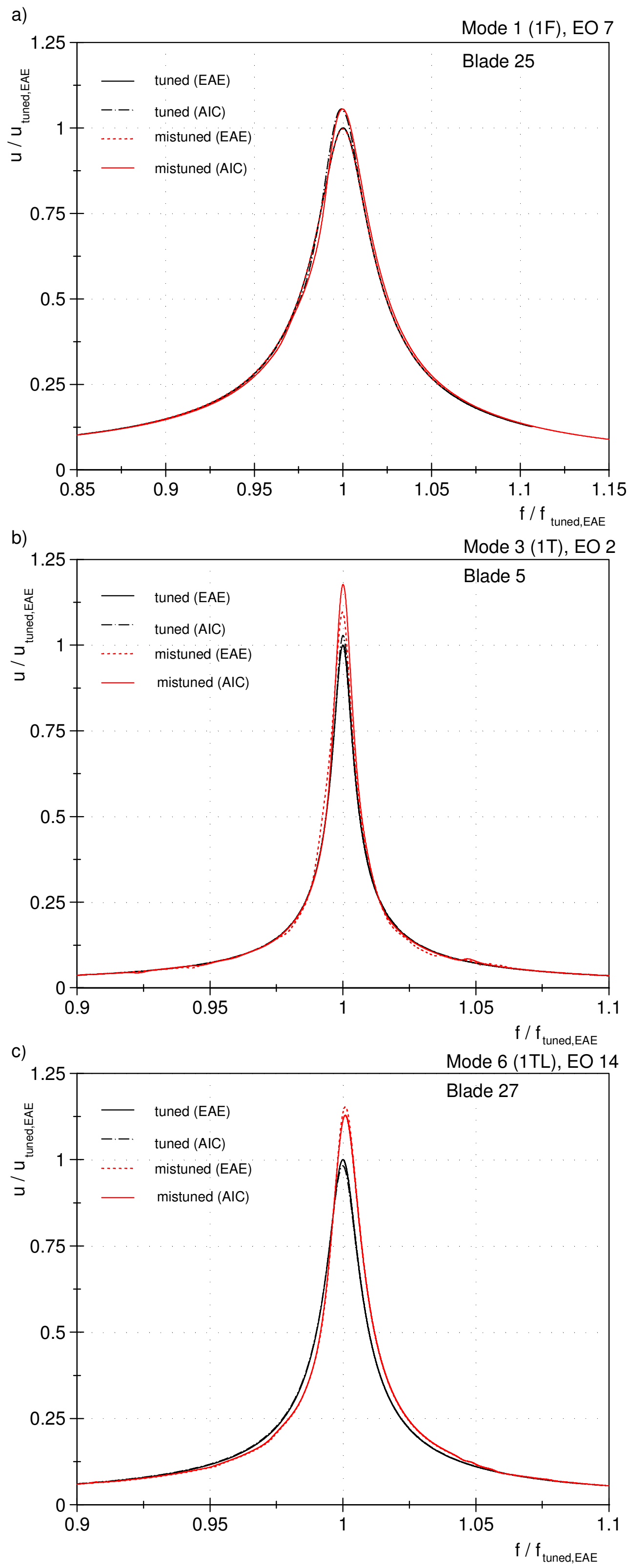

Figure 10: Frequency Response Functions (tuned and mistuned) a) Mode 1 b) Mode 3 c) Mode 6

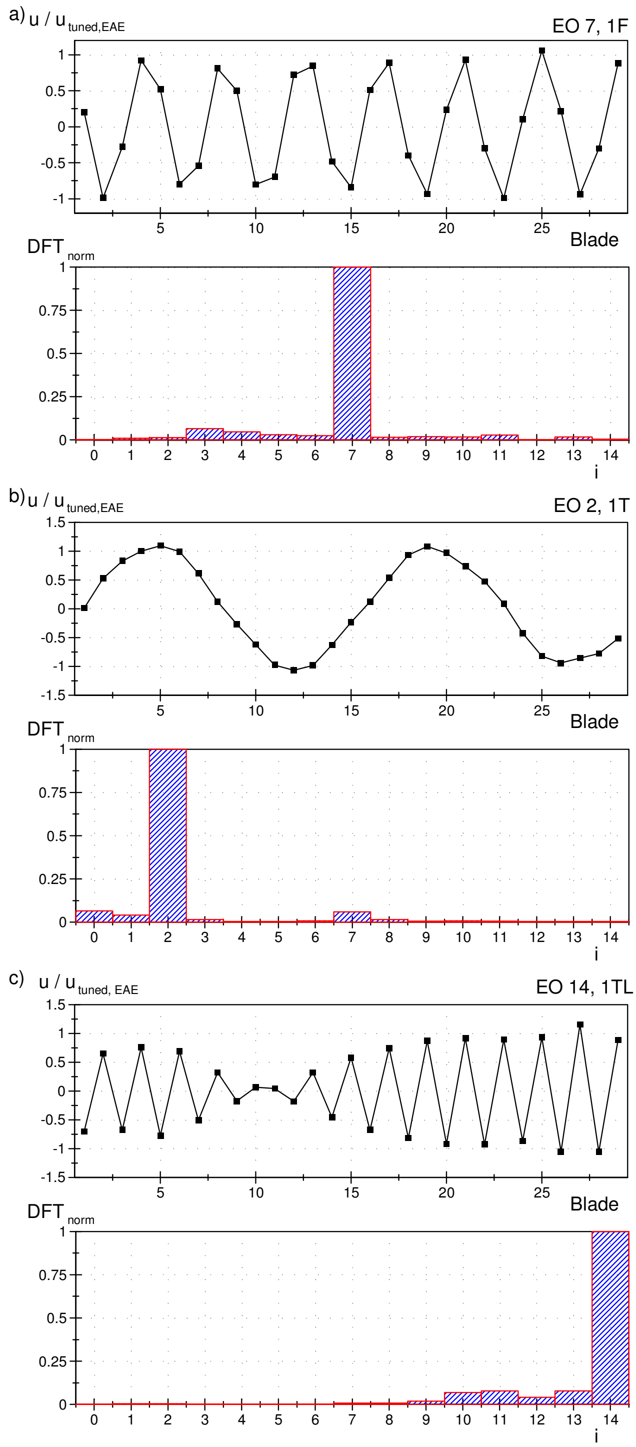

Figure 11: Modes of vibration at blades' DOF and fourier decomposition at resonance (mistuned)

a) Mode 1 b) Mode 3 c) Mode 6

Since the quantitative frequency mistuning of the present HPC front blisk is comparatively moderate – the blade to blade frequency deviations do not exceed 0.3 % – and the structural coupling is clearly higher compared to a rear blisk, the modes of vibration response at resonance are similar to the sine-shaped modes of an ideally tuned system (Fig. 11). The fourier decompositions given in Fig. 11, which are dominated by the coefficient assigned to the exciting EO, emphasize this good-natured behavior. The apparently distorted sine-shape given in Fig. 11 c results from the low number of sample points (29) to describe a 14 sine-wave shape [18].

The good-natured character of the response also reflects in comparatively low maximum amplification factors of the tuned response. For a Mode 1 (EO 7) excitation 5.6 % (AIC and EAE) has been computed, 9.6 % (EAE) and 14.4 % (AIC) for Mode 3 (EO 2) and finally 15.3 % (EAE) and 14.9 % (AIC) for Mode 7 (EO 14). Again, the largest deviations comparing both methods occur in case of Mode 3.

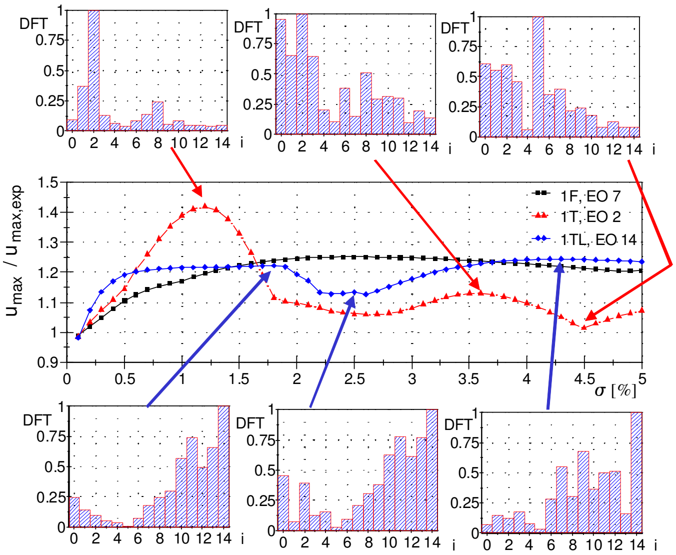

Figure 12: Maximum blade displacements (EAE-model) and selected fourier decompositions of modes at blades' DOF

Concluding, an analysis is considered addressing the question how the maximum blade response develops if the mistuning level is increased. For that purpose, the frequency mistuning distributions are scaled such that the relative distributions remain unchanged but the standard deviation is increased. In Figure 12 results are shown for the modes and EO-excitations as considered before starting from a standard deviation of 0.1 % up to 5 %. The original, experimentally determined distributions have been taken values around 0.12 %. It becomes apparent that increasing mistuning leads to growing displacements all in all. However, considering 1T and an EO 2-excitation, the initial increase at low standard deviations gets almost completely lost at σ = 4.5 %. The behavior can be explained with an increasing participation of other nodal diameter shapes at the vibration response due to the growing mistuning. In this case the fifth instead of the second nodal diameter shape dominates the response as to be seen in the fourier decompositions. Even if a possible decrease of the response [17, 19] due to strong mistuning, say more than 3 %, could not be proved in the present case, it could become possible in principle if the order of excitation is low and the aerodynamic damping of the associated nodal diameter mode is also low compared to higher nodal diameter modes.

7 CONCLUSIONS

The paper addresses a strategy to calculate forced responses of real blisks employing discrete low degree of freedom models introduced as equivalent blisk models (one for each blade mode) with a focus on the consideration of the fluid-structure interaction. Starting from a blade by blade frequency check by which mistuning is taken into account, the structural parts of the actual models are updated. Based on CFD-computations aerodynamic influence coefficients are calculated and included in the EBM, which is then ready for forced response simulations. In addition, aeroelastic eigenvalues are calculated and used as input to determine numerically discrete aerodynamic elements to be included in alternative EBMs. The motivation of such models results from the possibility to separate and assess the influences coming from the FSI in terms of co-vibrating air masses, air-stiffening and aerodynamic damping.

Comparing both the AIC- and the EAE-based EBM approach, an excellent correlation of the forced response simulations carried out here has been found for the fundamental blade mode of a moderately mistuned front HPC-blisk of the E3E-technology program. Apart from one exception still satisfying results at all, but increasing deviations are apparent for the first torsion and tramline mode with respect to the maximum displacements whereas differences in frequencies remain vanishingly low. In this context, a major influence comes along with the structural coupling of blades and disk. Considering the mistuned response, the aerodynamic coupling which is limited to immediately adjacent blades if the EAE-approach is applied, contribute to deviating results. A reduction of the mistuned response below the tuned one as shown in [17] and [19] could not be proved with the present case study.

Finally, it has to be mentioned that EBM-based analyses certainly cannot achieve the accuracy of fully coupled FE-based FSI-computations but contribute to enhance the understanding of the complex blisk vibration behavior. In this context the EBM should be regarded as useful tool to carry out sensitivity analyses.

ACKNOWLEDGMENTS

The work presented before has been supported by the Rolls-Royce Deutschland company. The authors thank for this commitment. The independent investigations contribute to the research project 'Life time maximization of blisks under consideration of the flow circulation' which is embedded in the graduate school ’Compressor Technologies & Materials’ with a funding by the Federal State of Brandenburg.

REFERENCES

[1] Ewins, D. J., 1969, “The Effects of Detuning Upon the Forced Vibrations of Bladed Disks”, Journal of Sound and Vibration, **9**, pp. 65-79.

[2] Griffin, J. H., Hoosac, T. M., 1984, “Model Development and Statistical Investigation of Turbine Blade Mistuning”, ASME Journal of Vibration, Acoustics, Stress, and Reliability in Design, **106**, pp. 204-210.

[3] Wei, S.-T., Pierre C., 1988, “Localization Phenomena in Mistuned Assemblies with Cyclic Symmetry Part I: Free Vibrations”, ASME Journal of Vibration, Acoustics, Stress, and Reliability in Design, **110**, pp. 429-438.

[4] Wei, S.-T., Pierre C., 1988, “Localization Phenomena in Mistuned Assemblies with Cyclic Symmetry Part II: Forced Vibrations”, ASME J. of Vibration, Acoustics, Stress, and Reliability in Design, **110**, pp. 439-449.

[5] Whitehead, D. S, 1998, “The Maximum Factor by Which Forced Vibration of Blades Can Increase Due to Mistuning”, ASME Journal of Engineering for Gas Turbines and Power, **120**, pp. 115-119.

[6] Petrov, E. P., Ewins, D. J., 2003, “Analysis of the Worst Mistuning Patterns in Bladed Disk Assemblies”, ASME Journal of Turbomachinery, **125**, pp. 623-631.

[7] Kenyon, J. A., Griffin, J. H., Feiner, D. M, 2003, “Maximum Bladed Disk Forced Response From Distortion of a Structural Mode”, ASME Journal of Turbomachinery, **125**, pp 352-363.

[8] Castanier, M. P., Pierre, C., 2006, “Modelling and Analysis of Mistuned Bladed Disk Vibration: Status and Emerging Directions”, Journal of Propulsion and Power, **22**, No. 2, pp. 384-396.

[9] Beirow, B., Kühhorn, A., Schrape, S., 2008, “A Discrete model to consider the influence of the air flow on blade vibrations of an integral blisk compressor rotor”, Proceedings of the ASME Turbo Expo 2008, Paper GT2008-50613, Berlin, Germany, June 9-13.

[10] Beirow, B., Kühhorn, A., Nipkau, J., 2009, “On the Influence of Strain Gauge Instrumentation on Blade Vibrations of Integral Blisk Compressor Rotors Applying a Discrete Model”, Proceedings of the ASME Turbo Expo 2009, Paper GT2009-59207, Orlando, FL, USA, June 8-12.

[11] Klinger, H., Lazik, W., Wunderlich, T., 2008, “The Engine 3E Core Engine”, Proceedings of the ASME Turbo Expo 2008, Paper GT2008-50679, Berlin, Germany, June 9-13.

[12] Strehlau, U., Kühhorn, A., 2010, “Experimental and numerical investigations of HPC blisks with a focus on travelling waves”, Proceedings of the ASME Turbo Expo 2010, Paper GT2010-22463, Glasgow, UK, June 14-18.

[13] Beirow, B., Kühhorn, A., Schrape, S., 2007, “Blisk Vibration Phenomena in Consideration of Fluid Structure Interaction . Proceedings of 11th International NAFEMS World Congress, Vancouver.

[14] Hanamura, Y, Tanaka, H. and Yamaguchi, K., 1980, “A simplified method to measure unsteady forces acting on the vibrating blades in cascade”. Bulletin of JSME, 23(180-12): 880–887.

[15] Kahl, G, 2002, “Aeroelastic Effects of Mistuning and Coupling in Turbomachinery Bladings”. Thèse N° 2629, École Polytechnique Fédérale de Lausanne.

[16] Kielb, R. E, Feiner, D, M., Griffin, J. H., Miyakozawa, T., 2004, „Flutter of mistuned bladed disks and blisks with aerodynamic and FMM structural coupling“, Proceedings of ASME Turbo Expo 2004, Paper GT2004-54315, Vienna, Austria.

[17] Nipkau, J, 2011, “Analysis of mistuned blisk vibrations using a surrogate lumped mass model with aerodynamic influences. Phd-thesis, Brandenburg University of Technology.

[18] Beirow, B., 2009, “Grundlegende Untersuchungen zum Schwingungsverhalten von Verdichterlaufrädern in Integralbauweise” (in German). Habilitation dissertation, Shaker, Aachen.

[19] Petrov, E. P., 2009, “A method for forced response analysis of mistuned bladed discs with aerodynamic effects included”, Proceedings of the ASME Turbo Expo 2009, Paper GT2009-59634, Orlando, FL, USA, June 8-12.

ANNEX A

BACKGROUND FOR THE DERIVATION OF EAE

Aiming to derive the EAE from aeroelastic eigenvalues the sector model (tuned, rigid disk) given in Fig. A1 is suited.

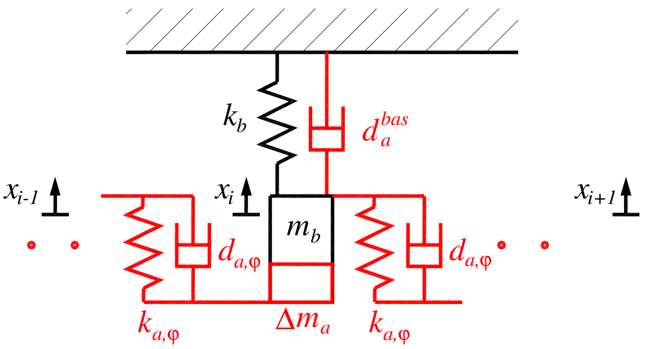

Figure A1: Sector model

Requiring equilibrium at the i^{th} DOF leads to

$$\left(\Delta m_{a,\varphi}+m_b\right)\ddot{x}_i+(d_a^{bas}+2d_{a,\varphi})\dot{x}_i-d_{a,\varphi}\left(\dot{x}_{i+1}+\dot{x}_{i-1}\right)+ \left(2k_{a,\varphi}+k_b\right)x_i-k_{a,\varphi}\left(x_{i+1}+x_{i-1}\right)=0 \qquad (A1)$$

Due to the cyclic symmetry of a tuned blisk there is a dependence of x_i on the adjacent DOF x_{i-1} and x_{i+1} according to

$$x_i=C_1x_{i-1}+C_2x_{i+1} \qquad (A2)$$

in which C_1 and C_2 are constants. In addition, the k^{th} DOF depends on the IBPA φ:

$$x_k=B\cos(\varphi_0+(k-i)\varphi) \qquad (A3)$$

with

$$k=1....\,i-1,\, i,\, i+1\, ,...,\, N.$$

B and φ_0 denote further constants. Aiming to determine C_1 and C_2 leads to

$$C_1B\cos[\varphi-\varphi_0]+C_2B\cos[\varphi+\varphi_0]=B\cos[\varphi_0] \qquad (A4)$$

or

$$C_1\{\cos[\varphi_0]\cos[\varphi]+\sin[\varphi_0]\sin[\varphi]\}+ C_2\{\cos[\varphi_0]\cos[\varphi]-\sin[\varphi_0]\sin[\varphi]\}=\cos[\varphi_0], \qquad (A5)$$

respectively. Equating coefficients results in

$$(C_1+C_2)\cos[\varphi]=1 \qquad (A6)$$

and

$$(C_1-C_2)\sin[\varphi]=0\,. \qquad (A7)$$

With that we get

$$C_1=C_2 \qquad (A8)$$

and with Eq. (A6)

$$2\cos[\varphi]=\frac{1}{C_1}\,. \qquad (A9)$$

Inserting Eq. (A9) in (A2) leads to

$$x_{i-1}+x_{i+1}=2\cos[\varphi]x_i \qquad (A10)$$

and considering Eq. (A1) finally to

$$(\Delta m_{a,\varphi}+m_b)\ddot{x}_i+(d_a^{bas}+2d_{a,\varphi}(1-\cos\varphi))\dot{x}_i+ (k_b+2k_{a,\varphi}(1-\cos\varphi))x_i=0 \qquad (A11)$$

or Eq. (11) with (12)-(14)

$$m_\varphi^*\ddot{x}_i+d_\varphi^*\dot{x}_i+k_\varphi^*x_i=0$$

respectively.

If forcing is employed on each blade i exciting a certain cyclic symmetry mode (CSM) according to

$$f_{\varphi,i}=\hat{f}_\varphi\cos(\Omega t+2\pi\cdot\mathrm{CSM}\frac{i}{N})\,, \qquad (A12)$$

the maximum displacement of each blade results in

$$\hat{x}_i=\hat{x}_0=\frac{\hat{f}_\varphi}{k_\varphi^*}V_\varphi^*\,. \qquad (A13)$$

From this we can derive

$$k_\varphi^*=\frac{\hat{f}_\varphi V_\varphi^*}{\hat{x}_0}\,. \qquad (A14)$$

This equation corresponds to Eq. (21), apart from a factor m_b, which becomes necessary since $\hat{f}_\varphi$ is computed as mass normalized modal force in the FSI-approach.